Supplementary Materials for

Substrate and product complexes reveal mechanisms of Hedgehog acylation by HHAT

Yiyang Jiang, Thomas L. Benz, Stephen B. Long*

*Corresponding author. Email: longs@mskcc.org

Published 11 June 2021, *Science* **372**, 1215 (2021)
DOI: 10.1126/science.abg4998

This PDF file includes:

Other supplementary material for this manuscript includes:

Materials and Methods

Cloning, expression and purification of HHAT

The cDNA encoding human HHAT (synthesized by IDT Inc.) was cloned into a mammalian expression vector with an N terminal EGFP tag and an intervening PreScission protease recognition site (*24, 25*). Wild type HHAT and all mutants were transiently expressed in HEK293T suspension cells (Invitrogen) that were cultured in Expi 293 media (Invitrogen) at 37°C with 8% CO_2 and 80% humidity. For transient transfection, cells were expanded into 1 liter cultures to a density of 2~3 × 10^6 cells/ml, at which point approximately 1 mg of plasmid was combined with 3 mg PEI25K (Polysciences, Inc. Cat # 23966) in 100 ml OptiMEM media (Invitrogen, and incubated at room temperature for 30 min) and the mixture was added to the cell culture. 5 mM sodium butyrate (final concentration) was added after 12 hours and the cells were cultured for an additional 48 hours before harvesting.

For purification of HHAT, the pellet from 1 liter of cells was resuspended in 50 ml extraction buffer (20 mM Tris, 300 mM NaCl, 10 mM lauryl maltose neopentyl glycol [LMNG, Anatrace], 40 μg/ml DNaseI, 1.5 μg/ml leupeptin, 1.5 μg/ml pepstatin A, 1 mM 4-benzenesulfonyl fluoride [AEBSF] and 1 mM benzamidine, pH 8.0) and solubilized by stirring at 4°C for 2 hours. The insoluble fraction was removed by centrifugation (60,000 g, 4°C, 45 min) and the supernatant was filtered through a 0.22 μm Millipore polystyrene membrane. 1.5 ml GFP nanobody resin was added and the sample was agitated at 4 °C for 2 hr (*26*). The beads were then washed with 40 ml of wash buffer (20 mM Tris, 300 mM NaCl, 1 mM LMNG, 10 μg/ml 1-palmitoyl-2-oleoyl-sn-glycero-3-phospho-L-serine [POPS, Avanti], pH 8.0) by gravity flow. HHAT was eluted by adding PreScission protease (0.1 mg, 6 hours at 4 °C) in elution buffer (20 mM Tris, 150 mM NaCl, 1 mM LMNG, 10 μg/ml POPS, 25 μM palmitoyl-CoA[preparing 25 mM stock in water, Sigma, Cat#P9716], 1 mM DTT, pH 8.0). The eluate was concentrated (100 kDa cutoff, to OD_{280} ~ 1) and flash frozen in liquid nitrogen (for enzymatic analysis) or further purified by size-exclusion chromatography (SEC, Superose-6 Increase, 10/300 GL column, GE Healthcare) in buffer (20 mM Tris, 150 mM NaCl, 0.06% [w/vol] digitonin [Cayman chemical], pH 8.0) prior to combining with Fab antibody fragments for cryo-EM studies, described below.

Antibody generation and purification of HHAT-Fab complexes

Monoclonal antibodies (designated 1C06 and 3H02) of isotype IgG1 were raised in mice by the Monoclonal Antibody Core Facility of the Memorial Sloan Kettering Cancer Center. Two antigens were used: HHAT that was purified in LMNG detergent, which yielded 1C06, and HHAT that had been reconstituted into nanodiscs (mMSP1D1, Cube Biotech Inc.), which yielded 3H02. The antibody selection process included ELISA, western blot, and fluorescence-detection size exclusion chromatography (FSEC) analysis (*27*) to identify antibodies that preferentially bound to native HHAT in comparison to SDS-denatured protein. IgG1 proteins were purified from hybridoma supernatants using affinity chromatography (HiTrap™ Protein G HP, Invitrogen) and Fab fragments were generated by ficin proteolysis (Pierce™ Mouse IgG1 Fab and F(ab')2 Preparation Kit, Thermo Scientific, Cat#44980), following the manufacturer's protocols. Fab fragments were further purified by anion exchange chromatography (Resource S column, GE Healthcare, in buffer 20 mM Sodium Acetate, 10 mM to 500 mM NaCl, pH 5.0) and then by SEC (Superdex 200 10/300 column, in 20 mM Tris, 150 mM NaCl, pH 8.0). For generation of HHAT-Fab complexes, purified antibodies were combined with purified ~ 0.1 mg/ml HHAT (using a molar ratio of 1:1.4, HHAT:Fab) and incubated at room temperature for 20 min. The samples were then concentrated to approximately 250 μl (using a 50 kDa Vivaspin 2 concentrator) and further purified by SEC (Superose-6 Increase, 5/10 column, GE Healthcare) in

20 mM Tris, 150 mM NaCl, 0.06% w/v Digitonin, pH 8.0. The elution fractions containing the HHAT-Fab complexes were pooled and concentrated (using a 50 kDa Vivaspin 2 concentrator).

Nanodisc reconstitution (used for antibody generation) was performed using an on-bead method analogous to that previously described (*25*). GFP-HHAT protein (from 500 ml of cell culture, corresponding to approximately 250 µg of purified HHAT) bound to 1 ml GFP-nanobody resin was combined with 80 µl lipid/DDM mixture (20 mM Tris, 150 mM NaCl, 14 mM DDM, 7.5 mg/ml POPC, 2.5 mg/ml POPE, 50 µg/ml POPS, 1 mg/ml lipid A, pH 8.0) and 100 µl mMSP1D1 (Cube Biotech Inc.**,** 5 mg/ml, in buffer 20 mM Tris-HCl, 100 mM NaCl, 5 mM sodium cholate, pH8.0). This yielded a molar ratio of approximately 1:4:160 (protein:mMSP1D1:lipid). After 1 h agitation at 4 °C, 500 mg of Bio-Beads (Bio-Rad, SM2, wet) were added to the resin, and the sample was rotated at 4 °C for detergent removal. Another 500 mg of Bio-Beads was added and the sample was incubated for 16 h (at 4 °C with rotation). The resin was then washed with 40 ml buffer (20 mM Tris, 150 mM NaCl, pH 8.0). The HHAT-nanodisc sample was eluted by adding 0.1 mg PreScission protease (6 h incubation at 4 °C in 3 ml of 20 mM Tris, 150 mM NaCl, 1 mM DTT, pH 8.0), further purified by SEC (Superose 6 increase, 10/300 GL column, GE Healthcare, equilibrated in 20 mM Tris, 150 mM NaCl, pH 8.0), concentrated to 1 mg/ml (50 kDa Vivaspin-2 concentrator), and used for immunization.

Cryo-EM sample preparation and data acquisition

For the palmitoyl-CoA substrate complex, 4 µl of freshly purified HHAT-1C06Fab-3H02Fab sample (at A_{280}=18.2) was loaded onto glow-discharged (10 s) Quantifoil R 1.2/1.3 carbon grids (Au 400, Electron Microscopy Sciences) and plunge-frozen in liquid nitrogen-cooled liquid ethane using a Vitrobot Mark IV plunge-freezing device (FEI, with 2.5 s blotting time at 4 °C, 0 blot force, and 100% humidity). Images were collected using SerialEM (*28*) using a Titan Krios microscope (Thermo, at MSKCC) at 300 kV that was equipped with a K3 summit direct electron detector (Gatan). Super-resolution movies (1.5 s exposure time; 60 frames per movie) were collected using a dose rate of 20 e^-/pixel/s at a nominal magnification of 22500× (super-resolution pixel size of 0.532 Å) and with defocus ranging from -0.7 µm to -2.5 µm.

For preparing the palmitoylated product complex, 1 mM DTT was added to the SEC-purified HHAT-3H02Fab sample after concentrating it to A_{280}=7.6. 4 µl of the complex was then supplemented with 0.5 µl of 25 mM palmitoyl-CoA (in water) and 0.5 µl of 20 mM Shh peptide (sequence: CGPGRGFGKRRK-biotin, synthesized by Peptide 2.0 Inc., 20 mM stock solution in 20 mM HEPES, 150 mM NaCl, 20 mM TCEP, pH 7.3) and the mixture was incubated on ice for 1 hour. The complete sample (5 µl) was used for grid preparation following the method described above. Images were collected using a Titan Krios3 microscope (Thermo, located at the New York Structural Biology Center) at 300 kV with a K3 electron detector (Gatan) and energy filter (BioQuantum, 20 eV filter width). Super-resolution movies (3 s exposure, 60 frames per movie) were collected with a dose rate of 17 e^-/pixel/s at a nominal magnification of 20,250× (super-resolution calibrated pixel size = 0.541 Å) with defocus ranging from -1.0 µm to -2.8 µm.

Structure determination and model building

Cryo-EM data processing workflows for the two datasets are summarized in figure S3 and followed the same scheme. Raw movies were motion-corrected using MotionCor2 (*29*). Micrograph defocus was estimated using CTFFIND-4.1 (*30*). Micrographs with estimated contrast transfer function (CTF) fits worse than 6 Å were discarded. Particles were autopicked in Relion 3.0 and extracted with 2x binning (*31*) and imported into CryoSPARC V2 for further processing (*32*). Particles that did not resemble HHAT antibody complexes were removed by reference-free 2D classification. Initial 3D models were generated ab initio. Particles were

selected by several rounds of heterogenous refinement. Classes yielding the highest resolution, as judged by density inspection and Fourier shell correlation (FSC), were selected for non-uniform refinement. Selected particles were then re-extracted without binning using Relion 3.0 and imported back to CryoSPARC V2 for additional rounds of heterogenous refinement. When the resolution no longer improved with rounds of heterogenous and non-uniform refinements, the particles were imported into Relion for Bayesian polishing, and then back into CryoSPARC V2 for non-uniform and CTF refinements. A second round of Bayesian polishing followed by non-uniform and CTF refinements yielded the final reconstructions at 2.68 Å or 3.20 Å resolutions for the palmitoyl-CoA and product complexes, respectively. All resolution estimates are based on gold-standard FSC calculations.

The atomic models were manually built and refined in real space using COOT (*33*). Further refinements were carried out by iterative cycles of real space refinement in PHENIX (*34*) and building in COOT. Structural figures were prepared with ChimeraX and Chimera (*35, 36*). Model quality was assessed using PHENIX and Molprobity (*37*). Electrostatic calculations used the APBS (*38*) plugin in Pymol (pymol.org).

Molecular dynamics simulation

The CHARMM-GUI (http://www.charmm-gui.org) *Membrane Builder* was used to generate the simulation system and GROMACS input files (*39-43*). The atomic model of HHAT (including the heme but without additional ligands) was uploaded to CHARMM-GUI via the "Bilayer Builder." HHAT was oriented in the lipid bilayer using the Orientations of Proteins in Membranes (OPM) PPM server (https://opm.phar.umich.edu/ppm_server)(*44*). The system size is approximately 103 × 103 × 108 $Å^3$ and ~ 108,000 atoms, including 21,537 water molecules, 99 sodium ions, 58 chloride ions, and 260 lipid molecules. The lipid bilayer is composed of 60% POPC, 15% POPE, 10% POPI, 10% cholesterol, and 5% POPS. GROMACS input and parameter files were created using the CHARMM36m force field (*45*), automatically-generated grid information for Particle-mesh Ewald (PME) fast Fourier transform (FFT) long-range interaction calculations, and the NPT equilibration ensemble (i.e., constant particle number, pressure and temperature) at 1 atm and 310 K (*45, 46*).

These CHARMM-GUI-generated input and parameter files were used for energy minimization, NPT equilibration, and molecular dynamics (MD) production simulation using GROMACS version 2020.2 (10.5281/zenodo.3773799) (*47*). Equilibration included 6 cycles of 50–100 ps each (1 fs time step) with reducing force constants with each subsequent cycle. The MD production was run for 90 ns (2 fs time step) using the Verlet cutoff scheme, Nose-Hoover temperature coupling, and Parrinello-Rahman pressure coupling. In the final trajectory, HHAT was re-centered and molecules were re-wrapped within the unit cell. For visualization, individual frames were least-squares fit to the protein backbone. Visual Molecular Dynamics (VMD; https://www.ks.uiuc.edu/Research/vmd/) was used to visualize the simulation and generate figures (*48*). Snapshots and the movie were rendered using Tachyon in VMD (*49*).

HHAT activity assay

In the standard assay, a biotin-labeled peptide (^{24}CGPGRGFGKRRK^{35}-biotin) corresponding to the N-terminal region of human Sonic Hedgehog after signal peptide removal was chemically synthesized (Peptide 2.0) and resuspended in buffer (20 mM stock in 20 mM HEPES, 150 mM NaCl, 20 mM TCEP, pH 7.3). For experiments with the R28A mutant peptide, a ^{24}CGPGAGFGKRRK^{35}-biotin peptide was used. Radiolabeled [^{3}H]palmitoyl-CoA was used to detect acyl transfer. The standard reaction mixture (50 µl) contains 10 nM HHAT (protein concentration determined from A_{280} for purified protein, or by GFP fluorescence for

microsomes), 50 μM palmitoyl-CoA (Sigma Aldrich, 25mM stock in H_2O), 40 nM [^{3}H]palmitoyl-CoA (60 Ci/mmol, American Radiolabeled Chemicals, Inc.) and 50 μM peptide in reaction buffer (150 mM MES at pH 6.5, 150 mM NaCl, 1 mM DTT, with 1 mM LMNG for detergent-solubilized HHAT or without detergent for microsomes). 5 nM HHAT (in detergent) was used for Fab inhibition studies. For substrate response curves the peptide and palmitoyl-CoA concentrations were varied as indicated in figure legends. Reactions were carried out at 37°C for 20 min and stopped by adding 400 μl ice-cold quench buffer (20 mM HEPES, 150 mM NaCl, 0.2% v/v Tween-20, pH 7.5). The peptide was captured using 20 μl streptavidin beads (Streptavidin Sepharose High Performance, GE Healthcare) with rotation at 4°C for 1 hour. The beads were then collected by centrifugation (using a Costar® Spin-X centrifuge tube filter, 3000 g, 2 min, at room temperature) and washed twice with 400 μl buffer (20 mM HEPES, 150 mM NaCl, pH 7.5). The beads were then resuspended with 100 μl of the same buffer and transferred into scintillation vials containing 5 ml scintillation fluid (Ultima Gold, PerkinElmer Life Sciences). [^{3}H]palmitoyl incorporation was determined by scintillation counting. Background levels were subtracted using reaction mixture controls without enzyme (when assaying purified protein) or with microsomes from untransfected cells. Enzymatic data are mean ± s.e.m. and derived from three or more independent experiments. Initial velocity curves were fitted to a Michaelis-Menten model: $Y = V_{max}X / (K_M + X)$, where Y is the initial velocity, X is the substrate concentration, V_{max} is the maximum enzyme velocity, and K_M is the concentration of half-maximal velocity. For substrate response curves, the concentration of the fixed substrate was 50 μM. For assaying the activity of HHAT mutants shown in Figure 4G, proteins were purified using GFP-nanobody affinity chromatography as described above and the protein concentration was estimated by A_{280} and by comparative western blot (using the 1C06 antibody).

To assess the ability of purified HHAT to palmitoylate Hedgehog protein, amino acids 24-197 of human Sonic Hedgehog were expressed and purified from *E. coli* as previously described (*8*) and the incorporation of [^{3}H]palmitate was measured using a similar assay. Reaction mixtures (50 μl) contained 10 nM purified HHAT, 50 μM palmitoyl-CoA, 40 nM [^{3}H]palmitoyl-CoA, and 40 μM Hedgehog protein in the standard reaction buffer (150 mM MES at pH 6.5, 150 mM NaCl, 1 mM DTT, 1 mM LMNG). Reactions were carried out at 37°C for 30 min. Reactions were stopped by the addition of 200 μl 5% w/v SDS and proteins were precipitated by the addition of 200 μl 37.5% w/v trichloroacetic acid (TCA). Following a 45 minute incubation on ice, precipitates were collected on filters by centrifugation (Costar® Spin-X centrifuge tube filters, 4000 g, 1 min, at room temperature). The filters were then washed twice with 300 μl of Solution 1 (2% SDS, 6% TCA) and once with 300 μl Solution 2 (6% TCA) to remove free palmitoyl-CoA. The filters were then transferred into scintillation vials containing 4 ml scintillation fluid (Ultima Gold, PerkinElmer Life Sciences) and [^{3}H]palmitate incorporation was determined by scintillation counting.

To assay the activity of HHAT in cell membranes, microsomes were prepared in the following manner. Cells from 200 ml of cell culture were pelleted (900 g), resuspended in 10 ml resuspension buffer (20 mM Tris, 300 mM NaCl, pH 8.0), and lysed by sonication on ice (20% nominal converter amplitude, 20 duty cycle, 4 min. using a Branson Sonifier 250A). Cell debris was removed by centrifugation (15,000 g, 4 °C, 30 min). Microsomes were then pelleted by centrifugation (70,000 g, 4 °C, 45 min), resuspended in 5 ml of resuspension buffer, aliquoted, frozen at -80 °C, and used in the enzyme assay. To quantify the amount of HHAT protein (in the form of a GFP-HHAT fusion protein) present in the microsomes, an aliquot of microsomes was solubilized in buffer containing detergent (20 mM Tris, 300 mM NaCl, 10 mM LMNG, pH 8.0).

The detergent-solubilized sample was then applied to an SEC column (Superose-6 Increase, 10/300 GL GE Healthcare, equilibrated in 20 mM Tris, 150 mM NaCl, 1 mM LMNG, 10 μg/ml POPS, pH 8.0) and the amount of GFP-HHAT protein was assessed from the fluorescence signal of the eluted GFP-HHAT peak (normalized using purified GFP as described (*50*)). For measuring the activity of archway mutants relative to the wild type enzyme (fig. S8), 10 nM HHAT, 20 μM palmitoyl-CoA and 50 μM peptide were used in the assay.

Thermostability, Fab binding, and heme assays

To assess the thermostability of wild type and C324V HHAT, 50 nM concentrations of purified proteins (in 20 mM Tris, 150 mM NaCl, 1 mM LMNG, 10 μg/ml POPS, pH 8.0) were incubated at temperatures ranging from 25 °C to 51 °C for 20 min and then analyzed by SEC (Superdex-200 10/300 GL column, GE Healthcare, equilibrated in the same buffer). The fraction of folded protein for each condition was quantified from the area under the elution peak (at ~13.7 ml, using tryptophan fluorescence: $\lambda_{excitation}$=280 nm, $\lambda_{emission}$=340 nm) in comparison to the peak of at 25 °C control sample.

To assess the approximate binding affinity of Fab 3H02, 2 nM of purified Fab was incubated (30 min at 20 °C) with concentrations of purified HHAT ranging from 0 to 100 nM in buffer (20 mM Tris, 150 mM NaCl, 1 mM LMNG, pH 8.0). Samples (500 μl) were then analyzed by SEC (Superdex-200 10/300 GL, GE Healthcare) in the same buffer. The fraction of unbound Fab was quantified from the area under the elution peak corresponding to free Fab (elution volume ~16.6 ml, using tryptophan fluorescence), which is well separated from the peaks for HHAT alone (~13.7 ml) and the HHAT-3H02Fab complex. The curve corresponds to fits of: fraction of Fab bound=$[HHAT]^h/(K_D{}^h+[HHAT]^h)$, K_D: dissociation constant, h: Hill coefficient, [HHAT]: concentration of HHAT.

A heme assay (Sigma-Aldrich, MAK316) was used to determine the amount of heme present in the purified HHAT sample according to the manufacturer's protocol. The assay detects the amount of heme from absorbance at 400 nm following addition of a Heme Reagent supplied with the assay. We generated a standard curve using the Heme Calibrator solution, which is also supplied with the assay. The amount of heme present in a 15 μM sample of purified HHAT was determined to be approximately 18 μM, consistent with a stoichiometric amount with the protein. As a control, 15 μM bovine serum albumin (Sigma-Aldrich, A9647) was measured to contain less than 0.1 μM heme.

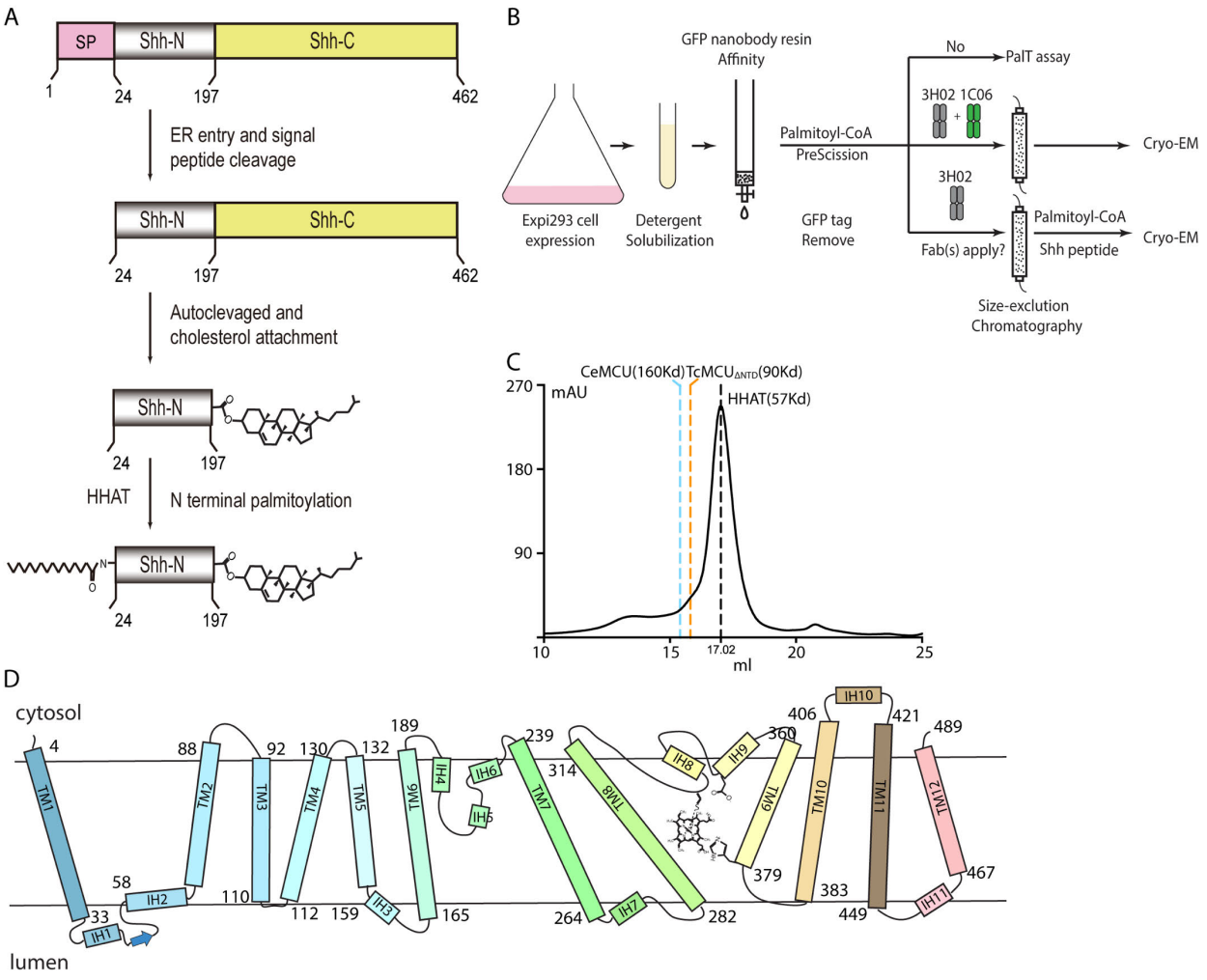

Figure S1. Hedgehog processing and HHAT biochemistry. (**A**) Sonic Hedgehog processing scheme. (**B**) Purification scheme for HHAT. (**C**) Size-exclusion chromatography (SEC) profile of purified HHAT in digitonin. Elution volumes of other purified membrane proteins from our laboratory are shown for comparison, with the total mass of these membrane proteins in parentheses. (**D**) Topology of HHAT determined from the structure, with coloring as in Figure 1C. Bars represent *α*-helices.

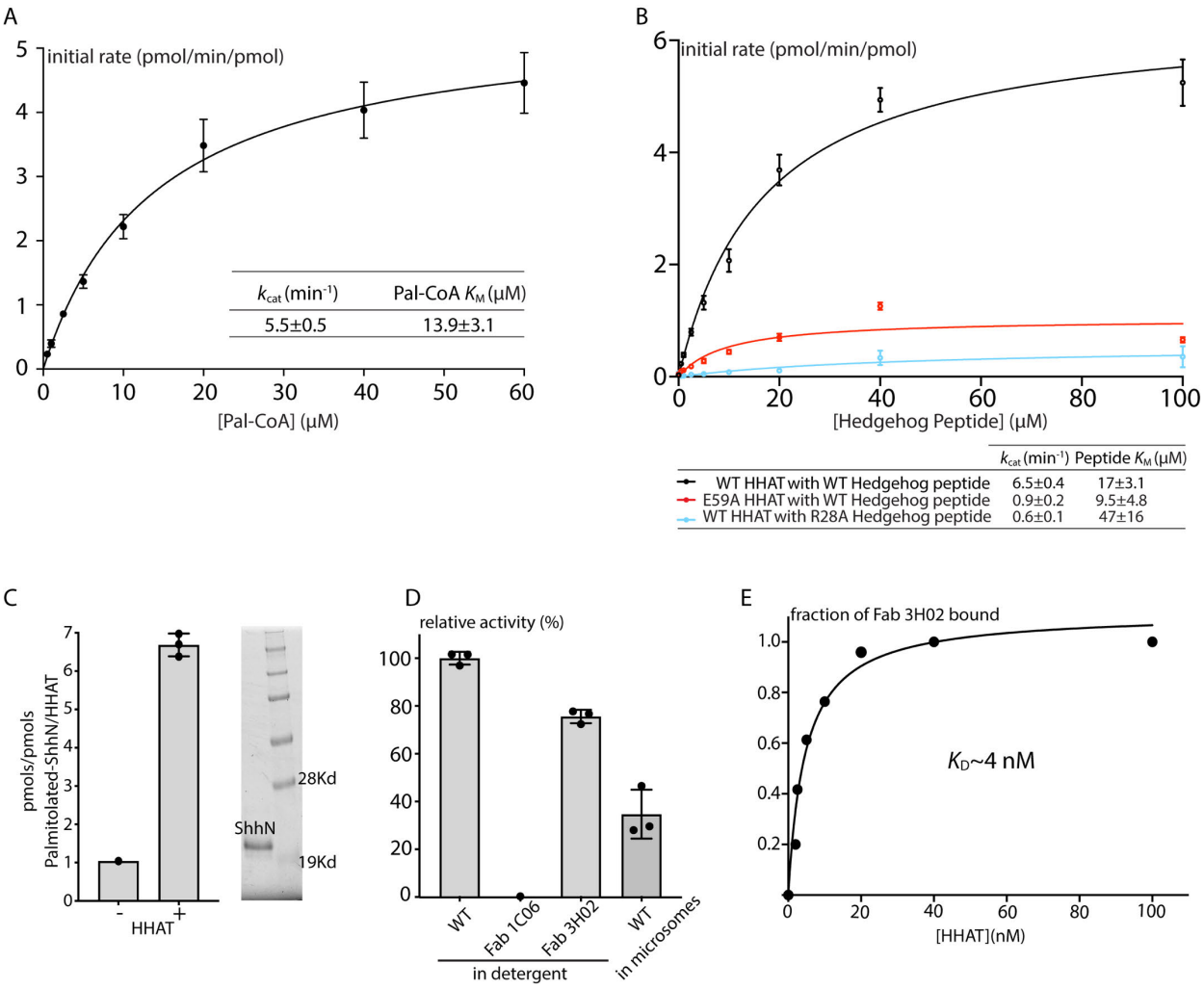

Figure S2. Enzymatic activity of HHAT and characterization of antibodies. (**A** and **B**) Enzymatic activities of purified wild type (WT) HHAT (or HHAT with a E59A mutation, as indicated) as functions of palmitoyl-CoA concentration (A) or wild type or E59A mutant Hedgehog peptide concentration (B). Michaelis-Menten fits are shown, mean ± s.e.m., with three independent experiments. (**C**) Palmitoylation of human Sonic Hedgehog protein (amino acids 24-197) catalyzed by HHAT. The amount of palmitate transferred to purified Sonic Hedgehog during a 30 min reaction per pmol of HHAT enzyme is shown. A control without enzyme is also indicated. Three independent experiments were performed. Details can be found in the methods. The right panel shows Coomassie-stained SDS-PAGE analysis of the purified Sonic Hedgehog protein, along with molecular weight markers. (**D**) Relative catalytic activities of HHAT (5 nM) in microsomes and in purified form, with and without 20 nM concentrations of the 1C06 and 3H02 antibodies. (**E**) Binding characterization indicates that 3H02 antibody binds tightly to the enzyme even though has minimal effect on catalytic activity.

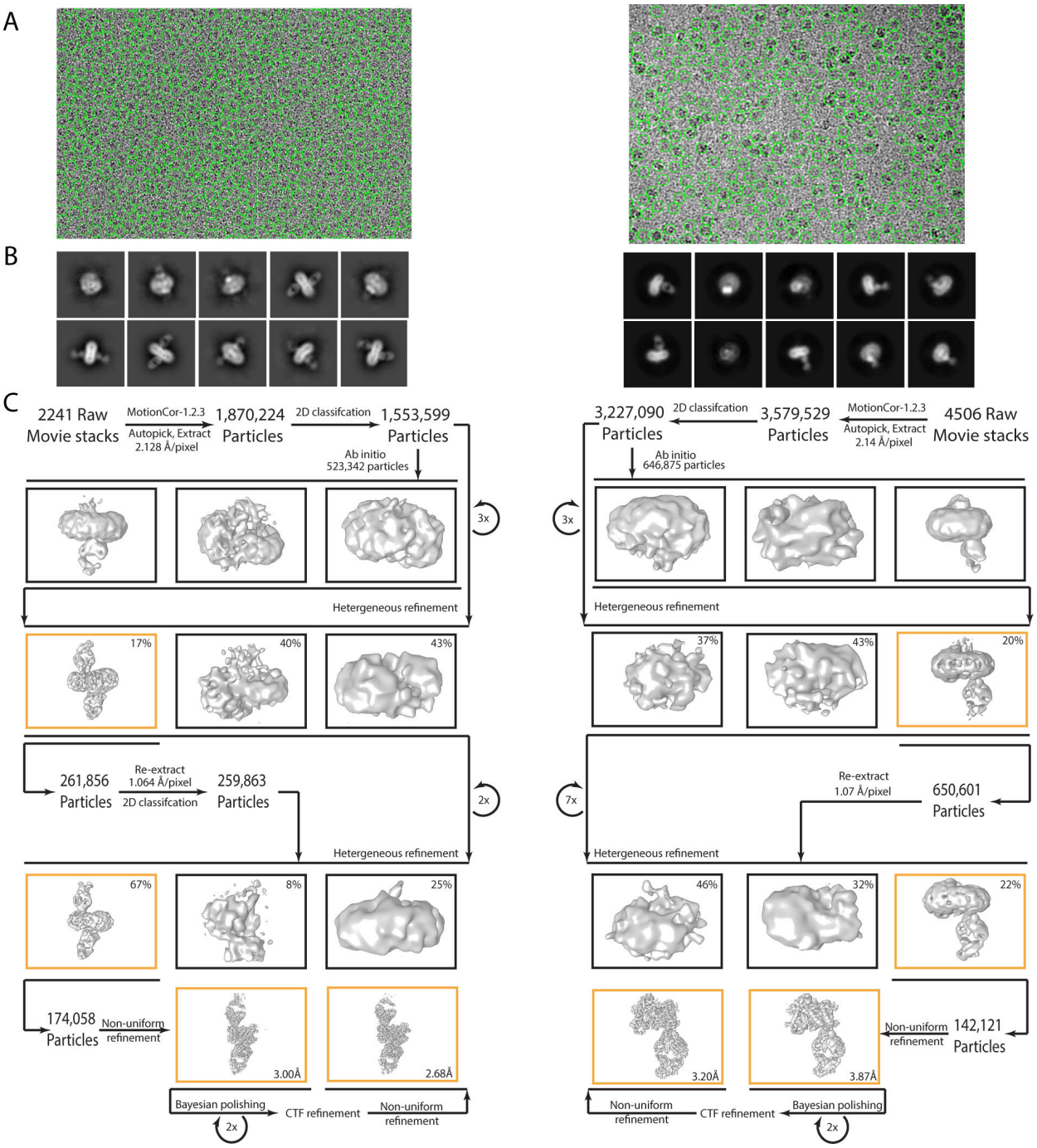

Figure S3. Cryo-EM data processing workflows for HHAT with palmitoyl-CoA (left) and with the palmitoylated peptide product complex (right). (**A**) Example cryo-EM micrographs, with picked particles circled. (**B**) 2D class averages of particles used for the final reconstructions. (**C**) Flow charts outlining the cryo-EM processing workflows. Details may be found in Methods.

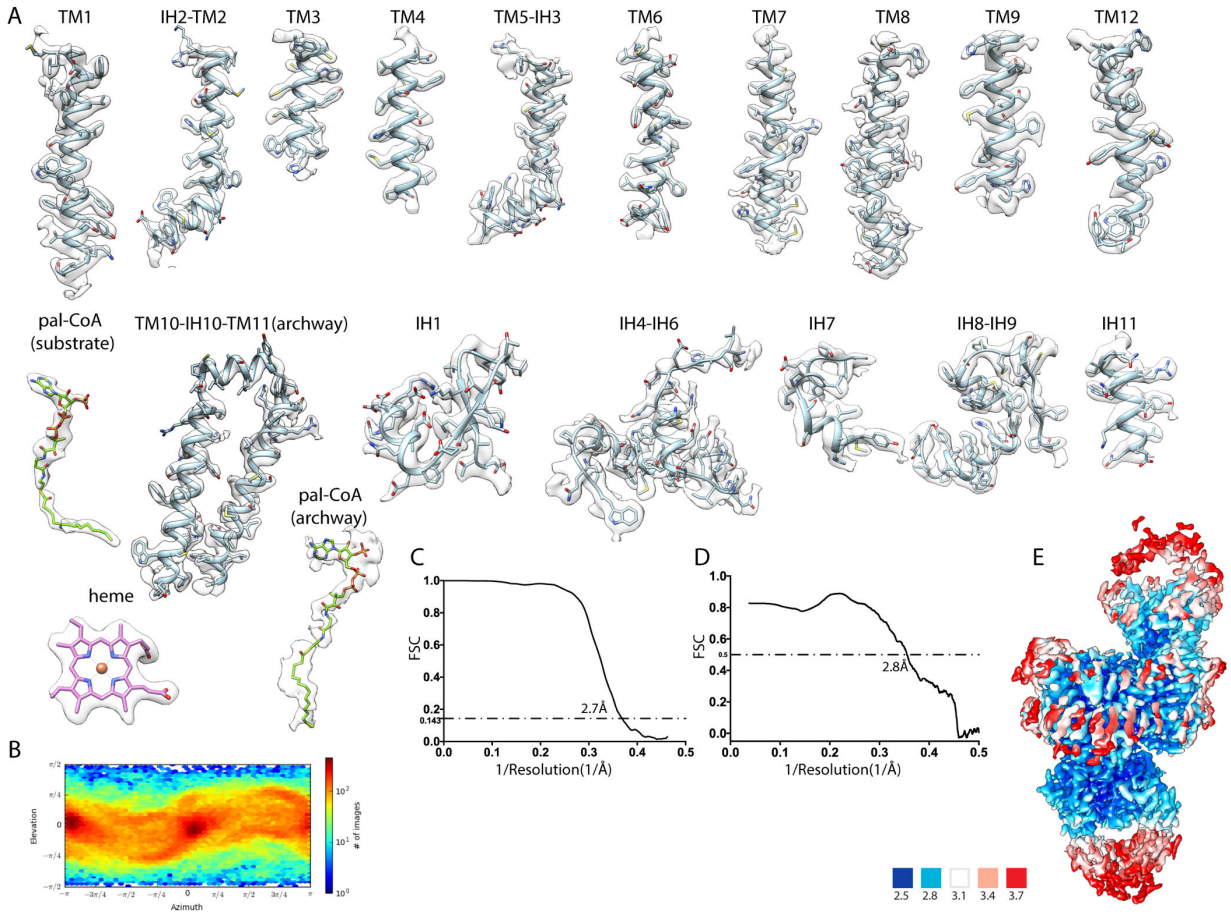

Figure S4. Density for the structure of HHAT with palmitoyl-CoA. (**A**) Densities (semi-transparent surface renderings) for indicated regions are shown in the context of the atomic model (sticks). (**B**) Angular distribution of particles used in the final cryo-EM reconstruction. (**C**) Gold-standard FSC curve of the final reconstruction. (**D**) Map-to-model correlation curve. (**E**) Estimation of the local resolution of the map, colored as indicated (calculated using CryoSPARC V2).

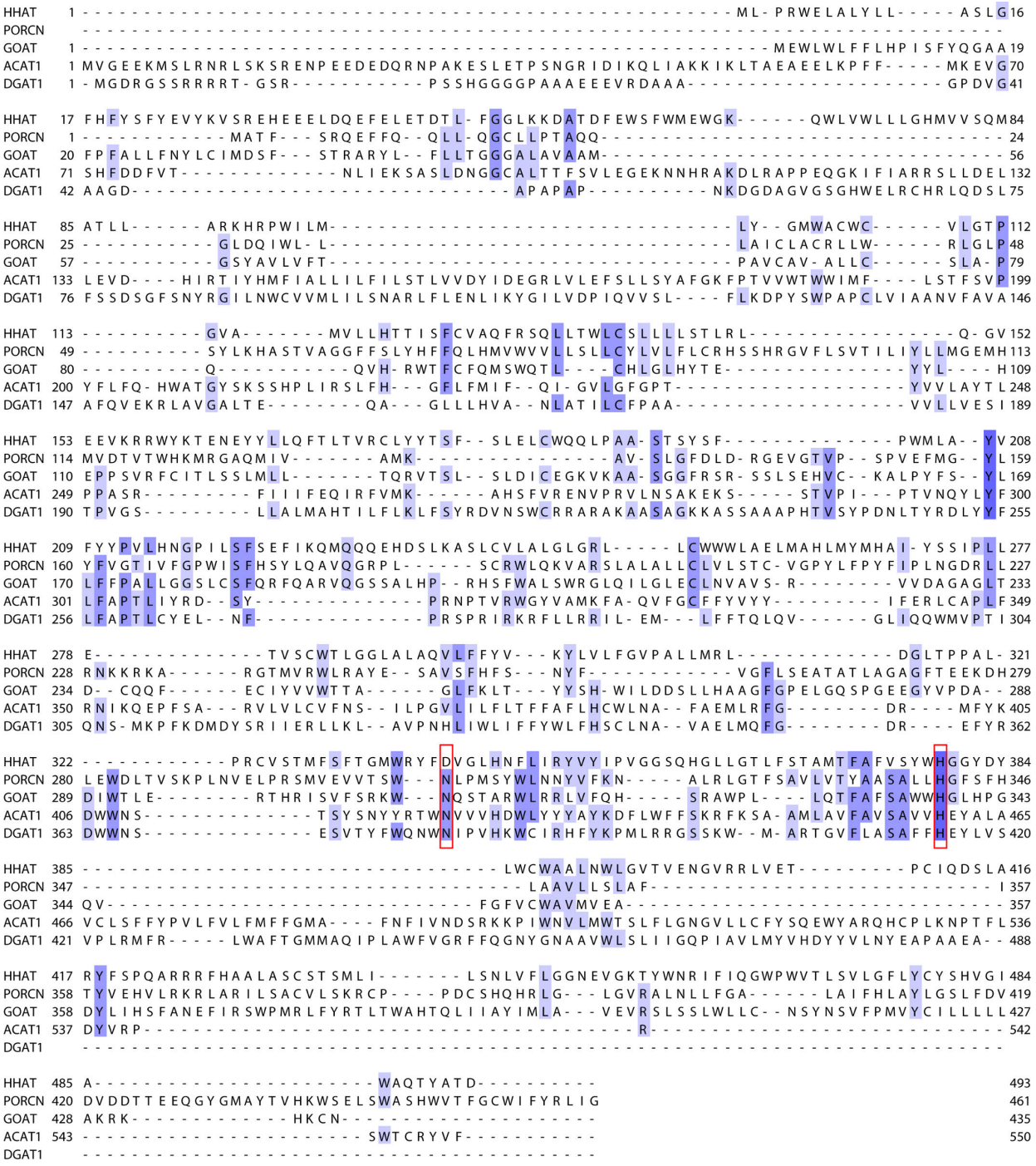

Figure S5. Sequence comparison among human MBOATs. The sequences of human HHAT, Porcupine, GOAT, ACAT1, and DGAT1 are aligned and colored according to sequence identity. Highly conserved polar residues implicated in catalysis (Asp 339 and His 379 in HHAT) are boxed in red.

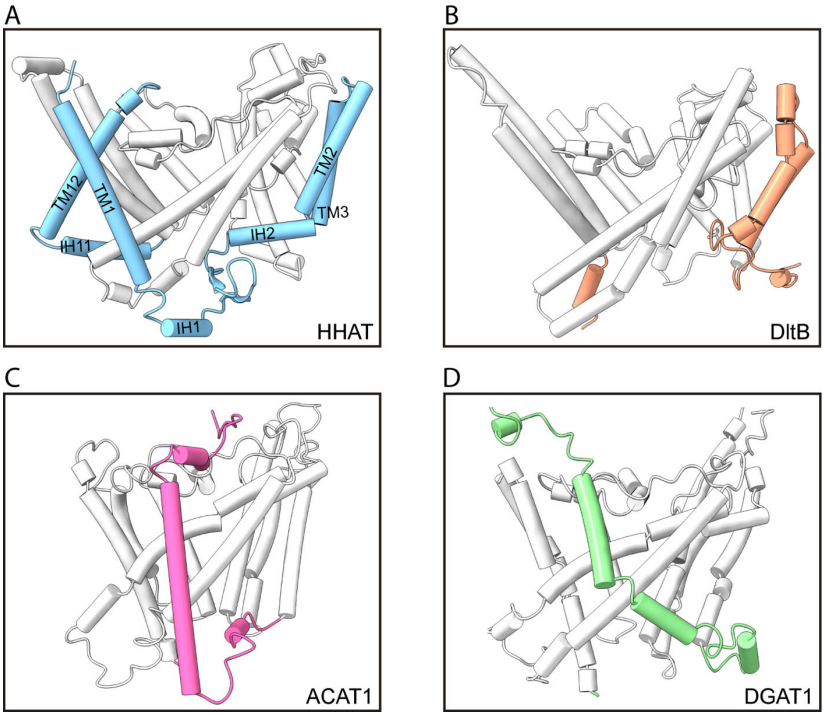

Figure S6. Comparison of HHAT with lipid-modifying MBOATs. (**A-D**) Structure of HHAT (A) in comparison to DltB (B) and monomers of ACAT1 (C) and DGAT1 (D) (*15-20*), with MBOAT fold domains in white and other regions in color.

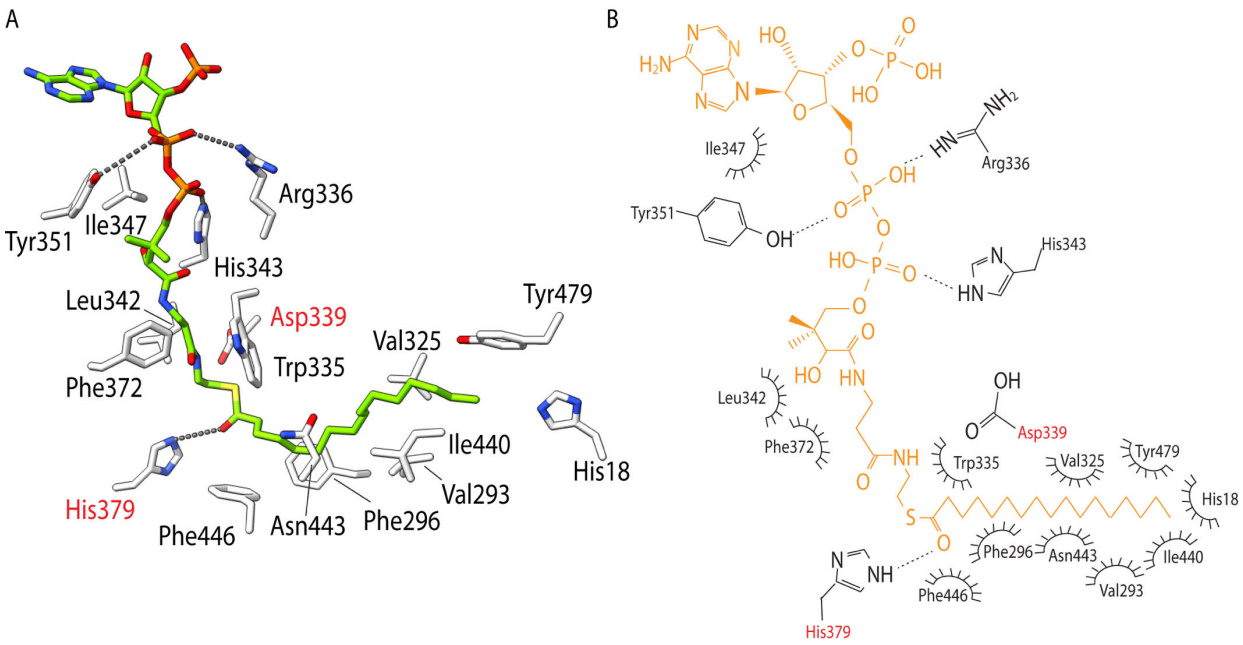

Figure S7. Interactions with palmitoyl-CoA in the substrate binding site. (**A**) Interacting residues shown as sticks, with hydrogen bonds denoted by dashes. (**B**) Schematic of the interactions. van der Waals interactions are shown as spiked arcs.

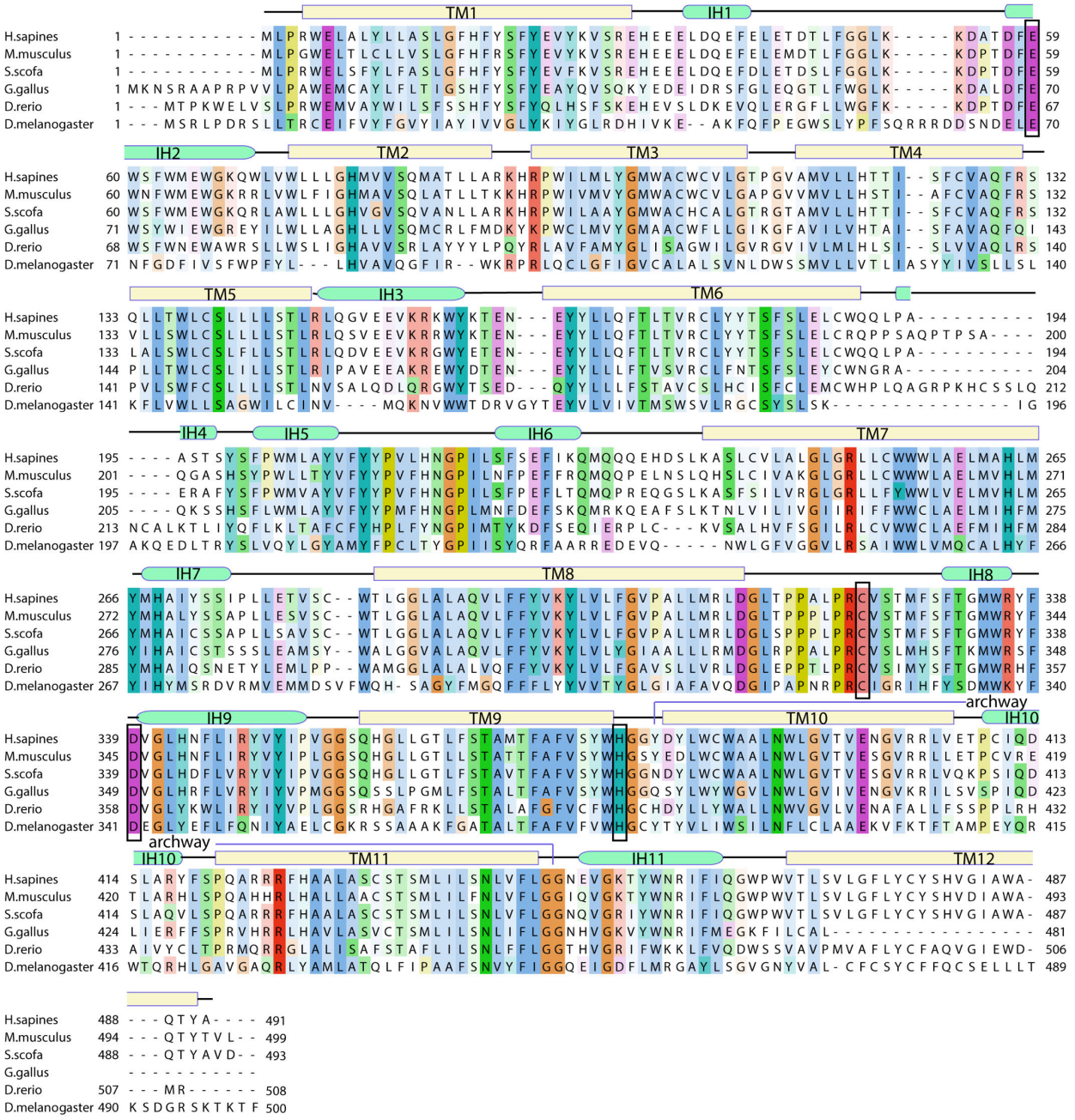

Figure S8. Sequence alignment of HHAT enzymes from various species. Secondary structural elements determined from the structure are positioned above the alignment, with helices shown as bars and loop regions as lines. Amino acids that when mutated to alanine dramatically reduced activity (Glu59, Cys324, Asp339 and His379) are denoted with black rectangles. The archway is labeled with brackets.

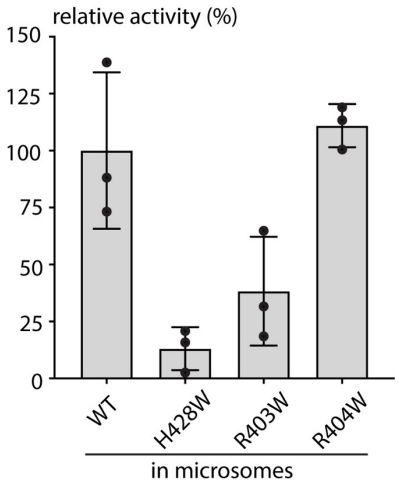

Figure S9. Relative enzymatic activity of the indicated mutants. His428 and Arg403 are located on the walls of the archway and contact palmitoyl-CoA there. Arg404 faces away from palmitoyl-CoA.

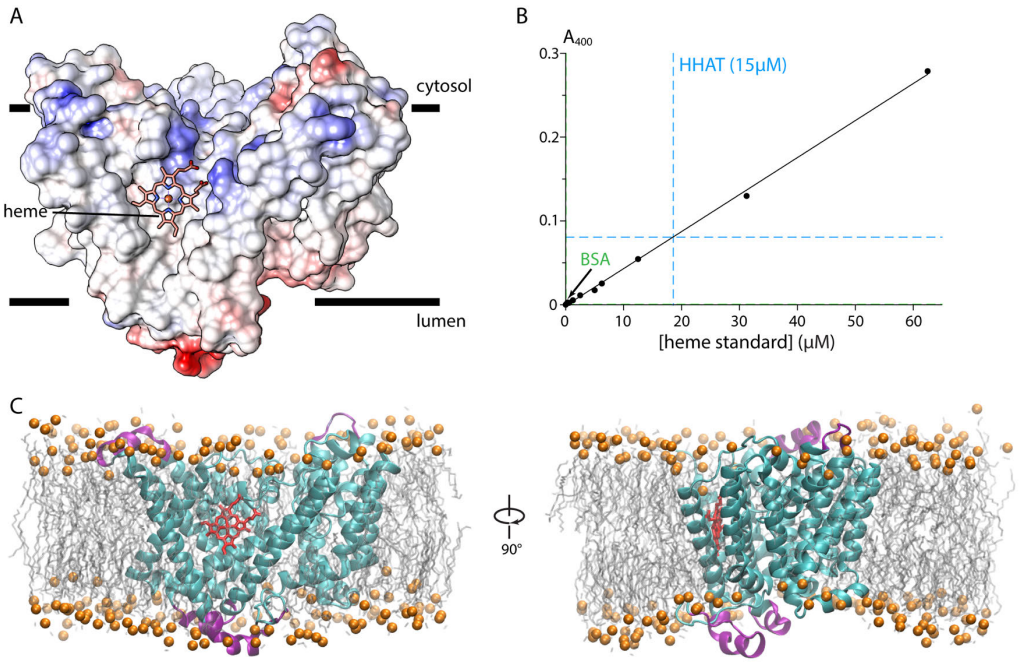

Figure S10. The heme is exposed to the membrane and a component of purified HHAT. (**A**) The molecular surface of HHAT shown from the side and colored according to electrostatic potential (light grey regions are neutral; red, −10 kT e^{-1}; blue, +10 kT e^{-1}). The heme is shown in stick representation. Approximate boundaries of the membrane are indicated by horizontal bars. The porphyrin ring of the heme is nearly co-planar with the central iron atom, indicative of a Fe(III) oxidation state (*51*). Its two propionate groups are oriented toward the cytosolic side where they form direct and water-mediated hydrogen bonds with Arg 250 and Arg 323, respectively (Fig. 3B). Although the heme does not contact the palmitoyl-CoA substrate, only a thin wall of protein separates it from the end of its acyl chain. (**B**) Biochemical assay showing that 15 μM purified HHAT contains approximately 18 μM heme (refer to Methods). 15 μM bovine serum albumin (BSA), used as a control, contains less than 0.1 μM heme. (**C**) Snapshot of an atomistic molecular dynamics simulation of HHAT in a lipid membrane, showing that the heme (red sticks) is in contact with lipid molecules (acyl chains shown as semi-transparent sticks; phosphate moieties as spheres). Regions of HHAT within the membrane's hydrophobic core are cyan; solvent-exposed regions are magenta. Two orthogonal perspectives are shown.

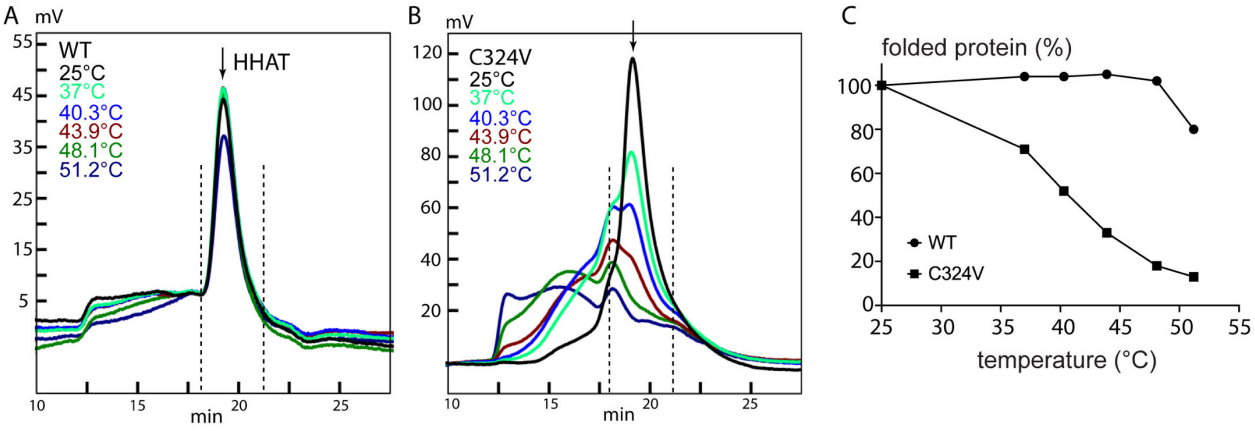

Figure S11. Thermal stability analyses of wild type and C324V HHAT. Purified wild type HHAT (**A**) or C324V HHAT (**B**) enzymes were incubated at the indicated temperatures and analyzed by SEC, measuring tryptophan fluorescence. The elution volume for properly folded HHAT is indicated by an arrow. Vertical lines indicate the region used to calculate the areas under the curves. (**C**) Quantification of folded protein following incubation at the indicated temperatures, determined from the areas under the curves indicated in (A) and (B).

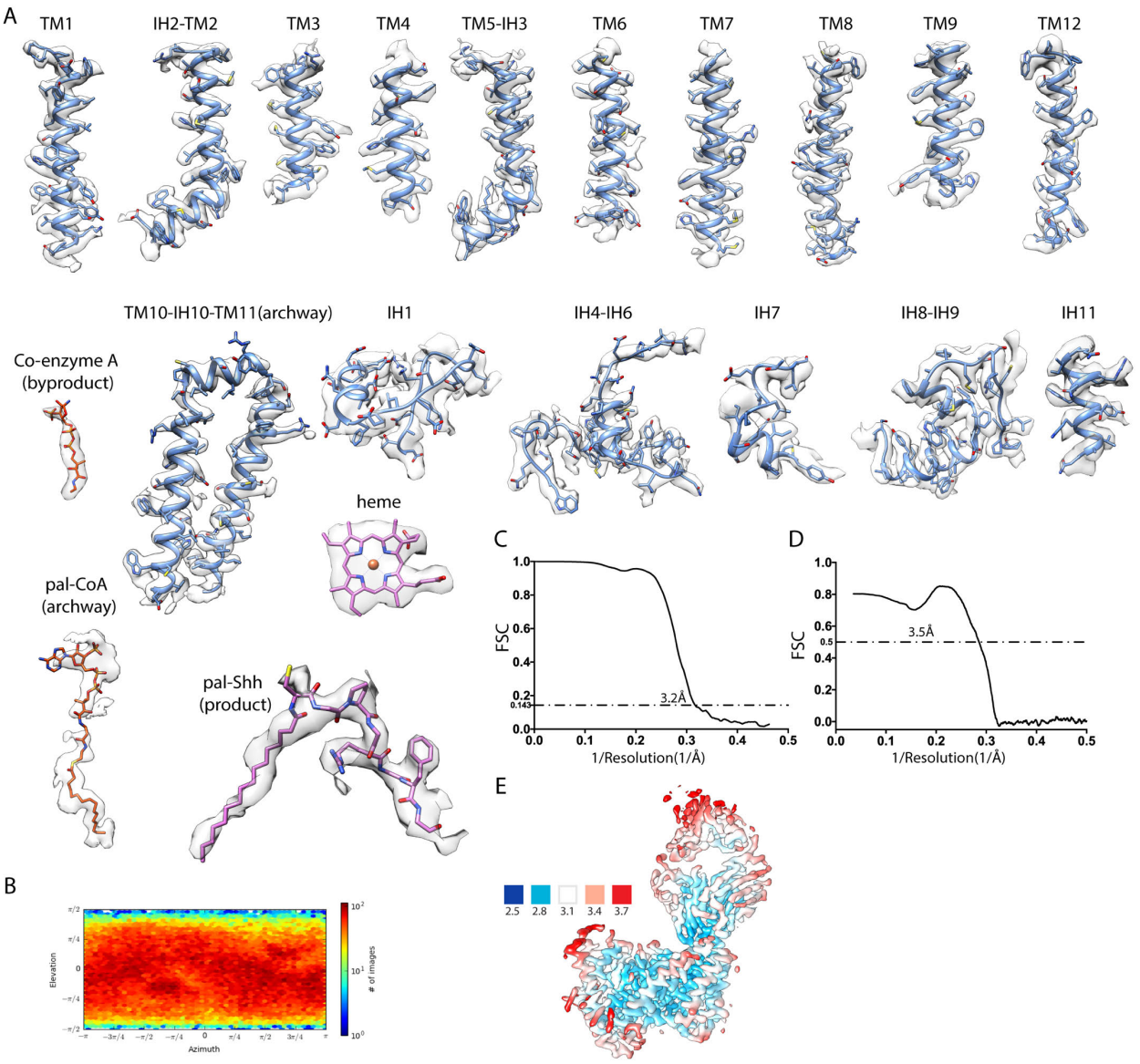

Figure S12. Density for the structure of HHAT with the palmitoylated peptide product. (**A**) Densities (semi-transparent surface renderings) for indicated regions are shown in the context of the atomic model (sticks). (**B**) Angular distribution of particles used in the final cryo-EM reconstruction. (**C**) Gold-standard FSC curve of the final reconstruction. (**D**) Map-to-model correlation curve. (**E**) Local map resolution estimation, colored as indicated (calculated using CryoSPARC V2).

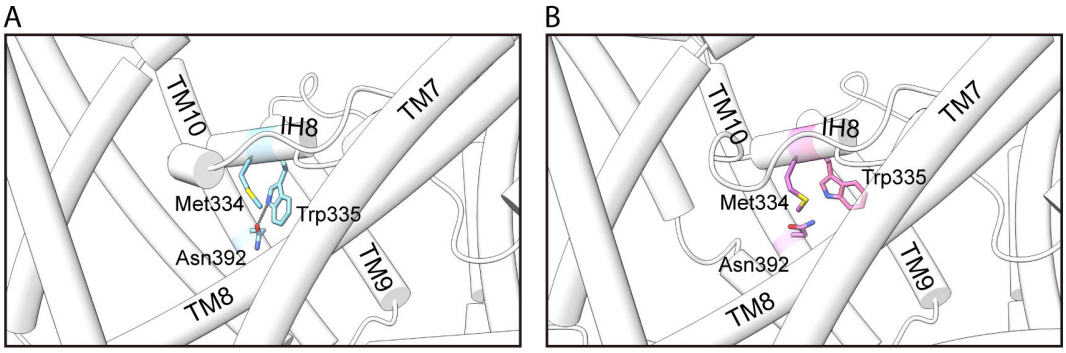

Figure S13. Rearrangement of Trp335 and concomitant rearrangements of Met334 and Asn392 between the substrate and product complexes. (**A, B**) Close up views of the HHAT-substrate complex (A) and HHAT-palmitoylated product complex (B) in the vicinity of Trp335, showing the conformations of Met334 and Asn392. A dashed line indicates a hydrogen bond.

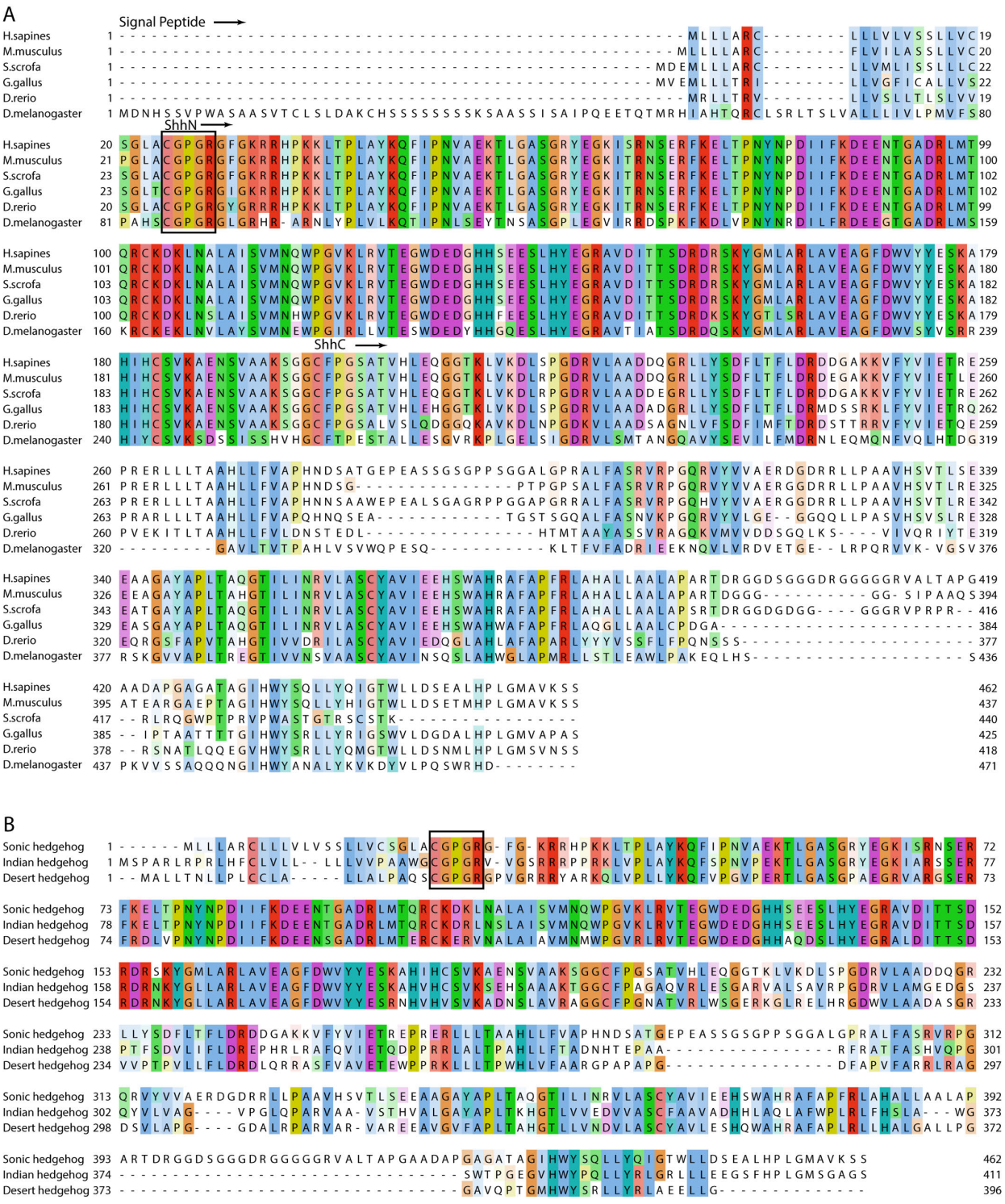

Figure S14. Sequence alignments of Hedgehog proteins. (**A**) Sequence alignment of Sonic Hedgehog proteins from the indicated species. (**B**) Alignment of human Sonic, Indian, and Desert Hedgehog proteins. A black rectangle indicates the N-terminal CGPGR sequence motif that is crucial for substrate recognition by HHAT.

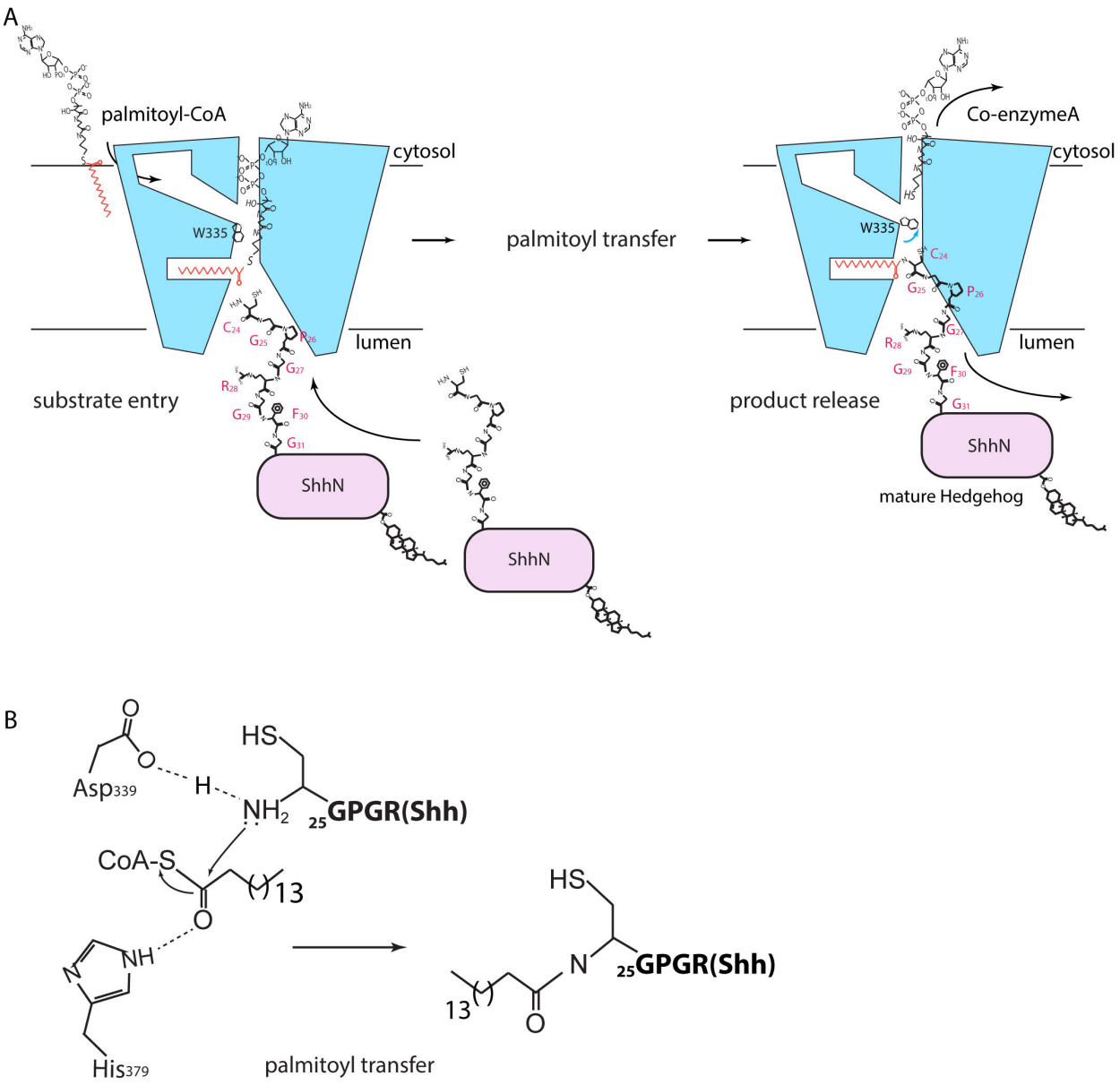

Figure S15. Proposed mechanism of HHAT. (**A**) Palmitoyl-CoA enters the reaction chamber from the cytosolic leaflet of the membrane by passing through the archway and then binds as a substrate deep within the enzyme. The amino terminal end of Hedgehog enters from the aqueous environment of the ER lumen. After palmitoyl transfer, the CoA byproduct is released into the cytosol and fully mature Hedgehog is released to the lumen. (**B**) Proposed chemical mechanism. Asp339 acts as a general base to activate the amino terminal end of Hedgehog for nucleophilic attack on the carbonyl carbon, thereby releasing CoA as the leaving group and forming the amide linkage of the fully mature Hedgehog product.

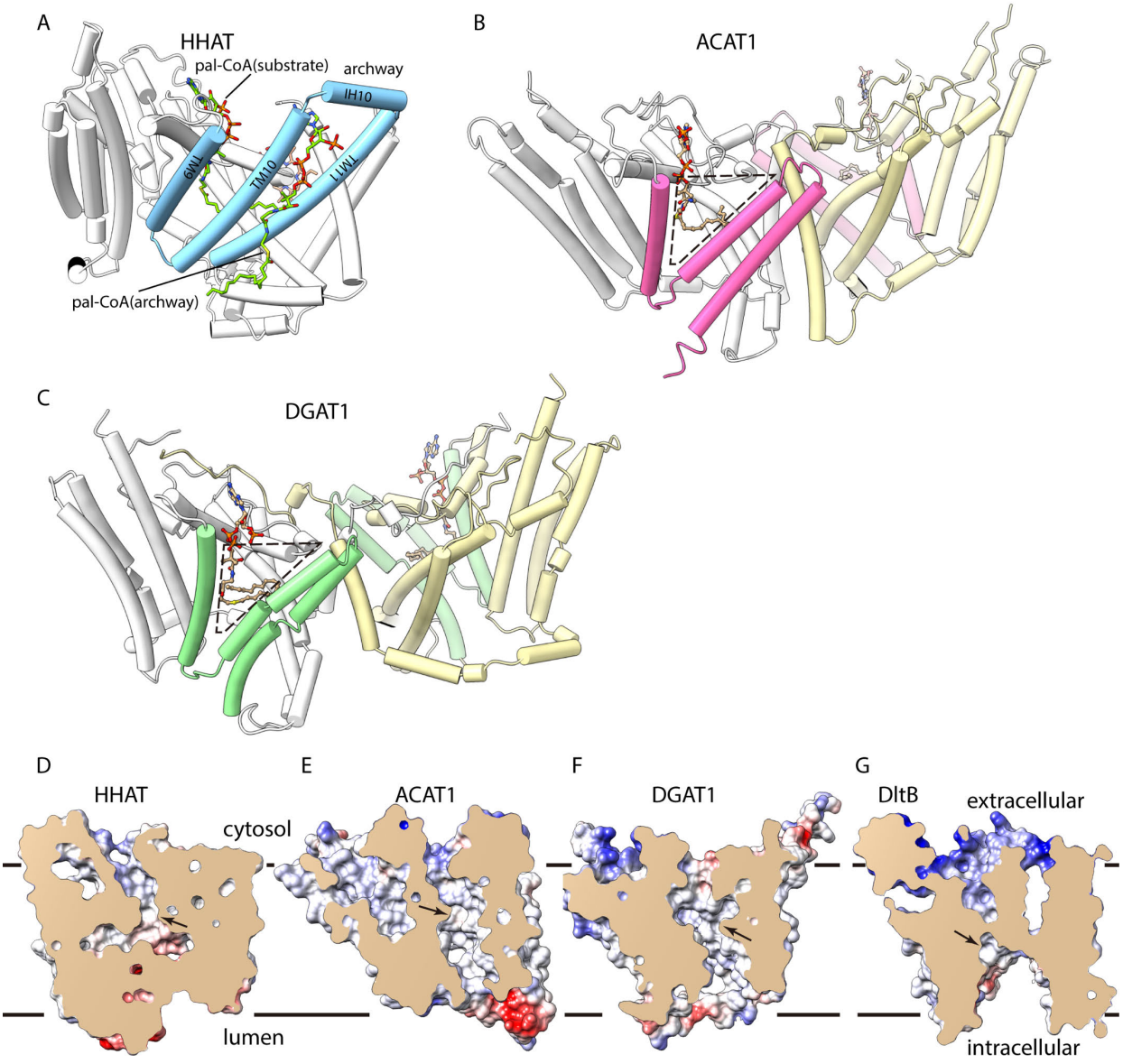

Figure S16. Substrate access routes for HHAT compared with lipid-modifying MBOATs. (**A-C**) Overall structure of HHAT (A) in comparison to the dimeric forms of ACAT1 (B) and DGAT1 (C) (*16-20*). TM9-TM11 of HHAT (A) is colored blue; the palmitoyl-CoA molecule in the archway is indicated. ACAT1 (B) and DGAT1 (C) do not possess an analogous archway. Rather, openings between transmembrane helices denoted by dashed triangles may serve as entry routes for their acyl-CoA substrates (*16-20*). (**D-G**) The active site of HHAT in comparison to the active sites of lipid-modifying MBOAT enzymes (*15-20*). Slices of the molecular surfaces highlight differences in their substrate binding cavities. Arrows indicate the location of the hallmark histidine residue in each enzyme. Monomers of ACAT1 and DGAT1 are shown.

	Palmitoyl-CoA substrate complex	Hedgehog peptide product complex
Data Collection		
Microscope	FEI Titan Krios-MSKCC	FEI Titan Krios-NYSBC(3)
Camera	Gatan K3	Gatan K3
Magnification	22,500	20,250
Voltage (kV)	300	300
Electron expose ($e^-/Å^2$)	26	53
Defocus range (μm)	-1.0 to -1.5	-1.2 to -2.2
Pixel size (Å)	1.064	1.083
Symmetry imposed	C1	C1
Initial particle images (No.)	1,870,224	3,579,529
Final particle images (No.)	174,058	142,121
Map Resolution (Å)	2.7	3.2
FSC threshold (0.143)		
Refinement		
Initial model used	*De novo*	Pal-CoA substrate complex
Model Resolution (Å)	2.8	3.5
FSC threshold (0.5)		
Model composition		
Non-hydrogen atoms	7904	6189
Protein residues	912	723
Ligands	18	15
Waters	15	0
Mean *B* factor ($Å^2$)		
Protein	43.9	110.64
Ligands	61.2	134.91
Water	32.1	-
R.m.s. deviation		
Bond lengths (Å)	0.007	0.004
Bond angles (°)	0.843	0.668
Validation		
Clashscore	8.09	8.12
Rotamers outlier (%)	0.54	0
Ramachandran plot		
Favored (%)	96.7	96.6
Allowed (%)	3.3	3.4
Disallowed (%)	0	0

Table S1. Cryo-EM data collection and model refinement statistics.

Movie S1. Molecular dynamics simulation of HHAT in a lipid membrane. The depiction is as in fig. S10C, showing the heme (red sticks) in direct contact with lipid molecules. Lipid molecules are represented as semi-transparent sticks for their acyl chains and spheres for their phosphate moieties. Regions of HHAT that reside within the hydrophobic core of the membrane are colored cyan whereas solvent-exposed regions are magenta.

References

1. F. Wu, Y. Zhang, B. Sun, A. P. McMahon, Y. Wang, Hedgehog Signaling: From Basic Biology to Cancer Therapy. *Cell Chem. Biol.* **24**, 252–280 (2017). doi:10.1016/j.chembiol.2017.02.010 Medline

2. Z. Chamoun, R. K. Mann, D. Nellen, D. P. von Kessler, M. Bellotto, P. A. Beachy, K. Basler, Skinny hedgehog, an acyltransferase required for palmitoylation and activity of the hedgehog signal. *Science* **293**, 2080–2084 (2001). doi:10.1126/science.1064437 Medline

3. R. K. Mann, P. A. Beachy, Novel lipid modifications of secreted protein signals. *Annu. Rev. Biochem.* **73**, 891–923 (2004). doi:10.1146/annurev.biochem.73.011303.073933 Medline

4. M. H. Chen, Y. J. Li, T. Kawakami, S. M. Xu, P. T. Chuang, Palmitoylation is required for the production of a soluble multimeric Hedgehog protein complex and long-range signaling in vertebrates. *Genes Dev.* **18**, 641–659 (2004). doi:10.1101/gad.1185804 Medline

5. X. Qi, P. Schmiege, E. Coutavas, J. Wang, X. Li, Structures of human Patched and its complex with native palmitoylated sonic hedgehog. *Nature* **560**, 128–132 (2018). doi:10.1038/s41586-018-0308-7 Medline

6. X. Qi, P. Schmiege, E. Coutavas, X. Li, Two Patched molecules engage distinct sites on Hedgehog yielding a signaling-competent complex. *Science* **362**, eaas8843 (2018). doi:10.1126/science.aas8843 Medline

7. E. Petrova, A. Matevossian, M. D. Resh, Hedgehog acyltransferase as a target in pancreatic ductal adenocarcinoma. *Oncogene* **34**, 263–268 (2015). doi:10.1038/onc.2013.575 Medline

8. J. A. Buglino, M. D. Resh, Hhat is a palmitoylacyltransferase with specificity for N-palmitoylation of Sonic Hedgehog. *J. Biol. Chem.* **283**, 22076–22088 (2008). doi:10.1074/jbc.M803901200 Medline

9. R. Y. Hardy, M. D. Resh, Identification of N-terminal residues of Sonic Hedgehog important for palmitoylation by Hedgehog acyltransferase. *J. Biol. Chem.* **287**, 42881–42889 (2012). doi:10.1074/jbc.M112.426833 Medline

10. K. Hofmann, A superfamily of membrane-bound O-acyltransferases with implications for wnt signaling. *Trends Biochem. Sci.* **25**, 111–112 (2000). doi:10.1016/S0968-0004(99)01539-X Medline

11. C. C. Chang, C.-Y. G. Lee, E. T. Chang, J. C. Cruz, M. C. Levesque, T.-Y. Chang, Recombinant acyl-CoA:cholesterol acyltransferase-1 (ACAT-1) purified to essential homogeneity utilizes cholesterol in mixed micelles or in vesicles in a highly cooperative manner. *J. Biol. Chem.* **273**, 35132–35141 (1998). doi:10.1074/jbc.273.52.35132 Medline

12. D. Hishikawa, H. Shindou, S. Kobayashi, H. Nakanishi, R. Taguchi, T. Shimizu, Discovery of a lysophospholipid acyltransferase family essential for membrane asymmetry and

diversity. *Proc. Natl. Acad. Sci. U.S.A.* **105**, 2830–2835 (2008). doi:10.1073/pnas.0712245105 Medline

13. K. H. Grzeschik, D. Bornholdt, F. Oeffner, A. König, M. del Carmen Boente, H. Enders, B. Fritz, M. Hertl, U. Grasshoff, K. Höfling, V. Oji, M. Paradisi, C. Schuchardt, Z. Szalai, G. Tadini, H. Traupe, R. Happle, Deficiency of PORCN, a regulator of Wnt signaling, is associated with focal dermal hypoplasia. *Nat. Genet.* **39**, 833–835 (2007). doi:10.1038/ng2052 Medline

14. J. Yang, M. S. Brown, G. Liang, N. V. Grishin, J. L. Goldstein, Identification of the acyltransferase that octanoylates ghrelin, an appetite-stimulating peptide hormone. *Cell* **132**, 387–396 (2008). doi:10.1016/j.cell.2008.01.017 Medline

15. D. Ma, Z. Wang, C. N. Merrikh, K. S. Lang, P. Lu, X. Li, H. Merrikh, Z. Rao, W. Xu, Crystal structure of a membrane-bound O-acyltransferase. *Nature* **562**, 286–290 (2018). doi:10.1038/s41586-018-0568-2 Medline

16. C. Guan, Y. Niu, S.-C. Chen, Y. Kang, J.-X. Wu, K. Nishi, C. C. Y. Chang, T.-Y. Chang, T. Luo, L. Chen, Structural insights into the inhibition mechanism of human sterol O-acyltransferase 1 by a competitive inhibitor. *Nat. Commun.* **11**, 2478 (2020). doi:10.1038/s41467-020-16288-4 Medline

17. T. Long, Y. Sun, A. Hassan, X. Qi, X. Li, Structure of nevanimibe-bound tetrameric human ACAT1. *Nature* **581**, 339–343 (2020). doi:10.1038/s41586-020-2295-8 Medline

18. H. Qian, X. Zhao, R. Yan, X. Yao, S. Gao, X. Sun, X. Du, H. Yang, C. C. L. Wong, N. Yan, Structural basis for catalysis and substrate specificity of human ACAT1. *Nature* **581**, 333–338 (2020). doi:10.1038/s41586-020-2290-0 Medline

19. X. Sui, K. Wang, N. L. Gluchowski, S. D. Elliott, M. Liao, T. C. Walther, R. V. Farese Jr., Structure and catalytic mechanism of a human triacylglycerol-synthesis enzyme. *Nature* **581**, 323–328 (2020). doi:10.1038/s41586-020-2289-6 Medline

20. L. Wang, H. Qian, Y. Nian, Y. Han, Z. Ren, H. Zhang, L. Hu, B. V. V. Prasad, A. Laganowsky, N. Yan, M. Zhou, Structure and mechanism of human diacylglycerol O-acyltransferase 1. *Nature* **581**, 329–332 (2020). doi:10.1038/s41586-020-2280-2 Medline

21. J. A. Buglino, M. D. Resh, Identification of conserved regions and residues within Hedgehog acyltransferase critical for palmitoylation of Sonic Hedgehog. *PLOS ONE* **5**, e11195 (2010). doi:10.1371/journal.pone.0011195 Medline

22. N. M. Broadway, R. J. Pease, G. Birdsey, M. Shayeghi, N. A. Turner, E. David Saggerson, The liver isoform of carnitine palmitoyltransferase 1 is not targeted to the endoplasmic reticulum. *Biochem. J.* **370**, 223–231 (2003). doi:10.1042/bj20021269 Medline

23. J. J. Asciolla, M. D. Resh, Hedgehog Acyltransferase Promotes Uptake of Palmitoyl-CoA across the Endoplasmic Reticulum Membrane. *Cell Rep.* **29**, 4608–4619.e4 (2019). doi:10.1016/j.celrep.2019.11.110 Medline

24. A. Goehring, C.-H. Lee, K. H. Wang, J. Carlisle Michel, D. P. Claxton, I. Baconguis, T. Althoff, S. Fischer, K. C. Garcia, E. Gouaux, Screening and large-scale expression of membrane proteins in mammalian cells for structural studies. *Nat. Protoc.* **9**, 2574–2585 (2014). doi:10.1038/nprot.2014.173

25. C. Wang, R. Baradaran, S. B. Long, Structure and Reconstitution of an MCU-EMRE Mitochondrial Ca^{2+} Uniporter Complex. *J. Mol. Biol.* **432**, 5632–5648 (2020). doi:10.1016/j.jmb.2020.08.013 Medline

26. A. Kirchhofer, J. Helma, K. Schmidthals, C. Frauer, S. Cui, A. Karcher, M. Pellis, S. Muyldermans, C. S. Casas-Delucchi, M. C. Cardoso, H. Leonhardt, K.-P. Hopfner, U. Rothbauer, Modulation of protein properties in living cells using nanobodies. *Nat. Struct. Mol. Biol.* **17**, 133–138 (2010). doi:10.1038/nsmb.1727 Medline

27. T. Kawate, E. Gouaux, Fluorescence-detection size-exclusion chromatography for precrystallization screening of integral membrane proteins. *Structure* **14**, 673–681 (2006). doi:10.1016/j.str.2006.01.013 Medline

28. D. N. Mastronarde, Automated electron microscope tomography using robust prediction of specimen movements. *J. Struct. Biol.* **152**, 36–51 (2005). doi:10.1016/j.jsb.2005.07.007 Medline

29. S. Q. Zheng, E. Palovcak, J.-P. Armache, K. A. Verba, Y. Cheng, D. A. Agard, MotionCor2: Anisotropic correction of beam-induced motion for improved cryo-electron microscopy. *Nat. Methods* **14**, 331–332 (2017). doi:10.1038/nmeth.4193 Medline

30. A. Rohou, N. Grigorieff, CTFFIND4: Fast and accurate defocus estimation from electron micrographs. *J. Struct. Biol.* **192**, 216–221 (2015). doi:10.1016/j.jsb.2015.08.008 Medline

31. J. Zivanov, T. Nakane, B. O. Forsberg, D. Kimanius, W. J. H. Hagen, E. Lindahl, S. H. W. Scheres, New tools for automated high-resolution cryo-EM structure determination in RELION-3. *eLife* **7**, e42166 (2018). doi:10.7554/eLife.42166 Medline

32. A. Punjani, J. L. Rubinstein, D. J. Fleet, M. A. Brubaker, cryoSPARC: Algorithms for rapid unsupervised cryo-EM structure determination. *Nat. Methods* **14**, 290–296 (2017). doi:10.1038/nmeth.4169 Medline

33. P. Emsley, B. Lohkamp, W. G. Scott, K. Cowtan, Features and development of Coot. *Acta Crystallogr. D* **66**, 486–501 (2010). doi:10.1107/S0907444910007493 Medline

34. D. Liebschner, P. V. Afonine, M. L. Baker, G. Bunkóczi, V. B. Chen, T. I. Croll, B. Hintze, L.-W. Hung, S. Jain, A. J. McCoy, N. W. Moriarty, R. D. Oeffner, B. K. Poon, M. G.

Prisant, R. J. Read, J. S. Richardson, D. C. Richardson, M. D. Sammito, O. V. Sobolev, D. H. Stockwell, T. C. Terwilliger, A. G. Urzhumtsev, L. L. Videau, C. J. Williams, P. D. Adams, Macromolecular structure determination using X-rays, neutrons and electrons: Recent developments in Phenix. *Acta Crystallogr. D* **75**, 861–877 (2019). doi:10.1107/S2059798319011471 Medline

35. T. D. Goddard, C. C. Huang, E. C. Meng, E. F. Pettersen, G. S. Couch, J. H. Morris, T. E. Ferrin, UCSF ChimeraX: Meeting modern challenges in visualization and analysis. *Protein Sci.* **27**, 14–25 (2018). doi:10.1002/pro.3235 Medline

36. E. F. Pettersen, T. D. Goddard, C. C. Huang, G. S. Couch, D. M. Greenblatt, E. C. Meng, T. E. Ferrin, UCSF Chimera—A visualization system for exploratory research and analysis. *J. Comput. Chem.* **25**, 1605–1612 (2004). doi:10.1002/jcc.20084 Medline

37. C. J. Williams, J. J. Headd, N. W. Moriarty, M. G. Prisant, L. L. Videau, L. N. Deis, V. Verma, D. A. Keedy, B. J. Hintze, V. B. Chen, S. Jain, S. M. Lewis, W. B. Arendall 3rd, J. Snoeyink, P. D. Adams, S. C. Lovell, J. S. Richardson, D. C. Richardson, MolProbity: More and better reference data for improved all-atom structure validation. *Protein Sci.* **27**, 293–315 (2018). doi:10.1002/pro.3330 Medline

38. N. A. Baker, D. Sept, S. Joseph, M. J. Holst, J. A. McCammon, Electrostatics of nanosystems: Application to microtubules and the ribosome. *Proc. Natl. Acad. Sci. U.S.A.* **98**, 10037–10041 (2001). doi:10.1073/pnas.181342398 Medline

39. S. Jo, T. Kim, W. Im, Automated builder and database of protein/membrane complexes for molecular dynamics simulations. *PLOS ONE* **2**, e880 (2007). doi:10.1371/journal.pone.0000880 Medline

40. S. Jo, T. Kim, V. G. Iyer, W. Im, CHARMM-GUI: A web-based graphical user interface for CHARMM. *J. Comput. Chem.* **29**, 1859–1865 (2008). doi:10.1002/jcc.20945 Medline

41. S. Jo, J. B. Lim, J. B. Klauda, W. Im, CHARMM-GUI Membrane Builder for mixed bilayers and its application to yeast membranes. *Biophys. J.* **97**, 50–58 (2009). doi:10.1016/j.bpj.2009.04.013 Medline

42. J. Lee, D. S. Patel, J. Ståhle, S.-J. Park, N. R. Kern, S. Kim, J. Lee, X. Cheng, M. A. Valvano, O. Holst, Y. A. Knirel, Y. Qi, S. Jo, J. B. Klauda, G. Widmalm, W. Im, CHARMM-GUI Membrane Builder for Complex Biological Membrane Simulations with Glycolipids and Lipoglycans. *J. Chem. Theory Comput.* **15**, 775–786 (2019). doi:10.1021/acs.jctc.8b01066 Medline

43. E. L. Wu, X. Cheng, S. Jo, H. Rui, K. C. Song, E. M. Dávila-Contreras, Y. Qi, J. Lee, V. Monje-Galvan, R. M. Venable, J. B. Klauda, W. Im, CHARMM-GUI Membrane Builder toward realistic biological membrane simulations. *J. Comput. Chem.* **35**, 1997–2004 (2014). doi:10.1002/jcc.23702 Medline

44. M. A. Lomize, I. D. Pogozheva, H. Joo, H. I. Mosberg, A. L. Lomize, OPM database and PPM web server: Resources for positioning of proteins in membranes. *Nucleic Acids Res.* **40**, D370–D376 (2012). doi:10.1093/nar/gkr703 Medline

45. J. Huang, S. Rauscher, G. Nawrocki, T. Ran, M. Feig, B. L. de Groot, H. Grubmüller, A. D. MacKerell Jr., CHARMM36m: An improved force field for folded and intrinsically disordered proteins. *Nat. Methods* **14**, 71–73 (2017). doi:10.1038/nmeth.4067 Medline

46. B. R. Brooks, C. L. Brooks 3rd, A. D. Mackerell Jr., L. Nilsson, R. J. Petrella, B. Roux, Y. Won, G. Archontis, C. Bartels, S. Boresch, A. Caflisch, L. Caves, Q. Cui, A. R. Dinner, M. Feig, S. Fischer, J. Gao, M. Hodoscek, W. Im, K. Kuczera, T. Lazaridis, J. Ma, V. Ovchinnikov, E. Paci, R. W. Pastor, C. B. Post, J. Z. Pu, M. Schaefer, B. Tidor, R. M. Venable, H. L. Woodcock, X. Wu, W. Yang, D. M. York, M. Karplus, CHARMM: The biomolecular simulation program. *J. Comput. Chem.* **30**, 1545–1614 (2009). doi:10.1002/jcc.21287 Medline

47. M. J. Abraham, T. Murtola, R. Schulz, S. Páll, J. C. Smith, B. Hess, E. Lindahl, GROMACS: High performance molecular simulations through multi-level parallelism from laptops to supercomputers. *SoftwareX* **1–2**, 19–25 (2015). doi:10.1016/j.softx.2015.06.001

48. W. Humphrey, A. Dalke, K. Schulten, VMD: Visual molecular dynamics. *J. Mol. Graph.* **14**, 33–38, 27–28 (1996). doi:10.1016/0263-7855(96)00018-5 Medline

49. J. E. Stone, K. L. Vandivort, K. Schulten, paper presented at the Proceedings of the 8th International Workshop on Ultrascale Visualization—UltraVis ’13 (2013).

50. M. M. Diver, S. B. Long, Mutational analysis of the integral membrane methyltransferase isoprenylcysteine carboxyl methyltransferase (ICMT) reveals potential substrate binding sites. *J. Biol. Chem.* **289**, 26007–26020 (2014). doi:10.1074/jbc.M114.585125 Medline

51. M. Sánchez, L. Sabio, N. Gálvez, M. Capdevila, J. M. Dominguez-Vera, Iron chemistry at the service of life. *IUBMB Life* **69**, 382–388 (2017). doi:10.1002/iub.1602